

Kardar-Parisi-Zhang scaling in the Hubbard model

Cătălin Pașcu Moca,^{1,2} Miklós Antal Werner,^{1,3,4} Angelo Valli,¹ Gergely Zaránd,^{1,3} and Tomaž Prosen⁵

¹*Department of Theoretical Physics, Institute of Physics,
Budapest University of Technology and Economics, Budafoki út 8., H-1111 Budapest, Hungary*

²*Department of Physics, University of Oradea, 410087, Oradea, Romania*

³*MTA-BME Quantum Dynamics and Correlations Research Group, Institute of Physics,
Budapest University of Technology and Economics, Budafoki út 8., H-1111 Budapest, Hungary*

⁴*Strongly Correlated Systems Lendület Research Group,
Wigner Research Centre for Physics, H-1525, Budapest, Hungary*

⁵*Department of Physics, Faculty of Mathematics and Physics,
University of Ljubljana, Jadranska 19, SI-1000 Ljubljana, Slovenia*

(Dated: June 21, 2023)

We explore the Kardar-Parisi-Zhang (KPZ) scaling in the one-dimensional Hubbard model, which exhibits global $SU_c(2) \otimes SU_s(2)$ symmetry at half-filling, for the pseudo-charge and the total spin. We analyze dynamical scaling properties of high temperature charge and spin correlations and transport. At half-filling, we observe a clear KPZ scaling in both charge and spin sectors. Away from half-filling, the $SU_c(2)$ charge symmetry is reduced to $U_c(1)$, while the $SU_s(2)$ symmetry for the total spin is retained. Consequently, transport in the charge sector becomes ballistic, while KPZ scaling is preserved in the spin sector. These findings confirm the link between non-abelian symmetries and KPZ scaling in the presence of integrability. We study two settings of the model: one involving a quench from a bi-partitioned state asymptotically close to the $T = \infty$ equilibrium state of the system, and another where the system is coupled to two markovian reservoirs at the two edges of the chain.

I. INTRODUCTION

Universality, a crucial concept in statistical physics, refers to the similar behavior exhibited by diverse physical systems, despite having different microscopic details. This allows us to predict the behavior of complex physical systems based on a few universal characteristics instead of relying on the specifics of each system [1, 2]. In this context, originally, the KPZ (Kardar-Parisi-Zhang) universality class refers to a broad range of classical stochastic growth models that exhibit similar scaling behavior to the original KPZ equation [3–6]. These models describe the evolution of interfaces between two media, such as the growth of a crystal or the motion of a fluid [7, 8]. The key insight of the KPZ scaling is that the fluctuations at the interface exhibit a self-similar behavior, such that their statistical properties are invariant under rescaling of time and space.

The KPZ scaling has also been shown to describe high-temperature dynamics of certain many-body systems near equilibrium [9], building on previous observations [10–12]. This opened up new avenues for understanding the behavior of quantum many-body systems [13], allowed to identify commonalities between classical and quantum systems [11, 14–16], and provided a new framework for describing the complex dynamics of quantum quenches [9]. Through extensive investigations of near equilibrium dynamics of magnetization and spin currents in XXZ spin chains, it has been found that, exactly at the $SU(2)$ symmetric fixed point (i.e., associated with no anisotropy of the spin interaction) the dynamical spin structure factor can be exactly described by the KPZ correlation function, and thus exhibits superdiffusive behavior with dynamical scaling exponent $z = 3/2$. However, away from

this point, the system exhibits either ballistic or diffusive behavior [17]. Extensions to higher spin integrable models has been discussed as well [18, 19]. It has thus been conjectured [18] that high-temperature dynamical two-point correlation functions of Noether charges of all integrable systems with non-abelian symmetries are described by the Prähofer-Spohn [20] scaling function of KPZ universality class. The numerical [21–26] and experimental [27–29] evidence for the above conjecture has been mounting, whereas the proof or precise mechanism for its validity are still lacking. There has been, however, a clear self-consistent explanation of anomalous scaling exponent $z = 3/2$ within the framework of generalized hydrodynamics [30, 31] (see also review [32]). Nevertheless, there remains a crucial distinction between KPZ scaling in non-abelian integrable spin chains, and classical KPZ universality e.g. in surface growth phenomena. While the latter is clearly far from equilibrium and violating detailed balance, the former belongs to the domain of equilibrium physics. As such, distribution of fluctuations (i.e. full counting statistics) has to be symmetric and hence cannot be described by KPZ universality [33–35]. Therefore, more work is needed to understand even phenomenologically to what extent KPZ universality applies to non-abelian integrable spin chains.

So far, most studies have focused on spin models, and relatively less attention has been paid to non-abelian integrable fermionic models, such as the Hubbard model [36, 37]. The Hubbard model is a widely studied model in condensed matter physics and describes interacting fermions on a lattice with a local (on-site) repulsion [38]. At general fillings, the Hubbard model has a global $U_c(1) \otimes SU_s(2)$ symmetry associated with the total charge (c) and spin (s) conservation. As we discuss

it in detail in Sec. II, the global symmetry is raised to $SU_c(2) \otimes SU_s(2)$ at half filling, which makes the Hubbard model a particularly interesting candidate for investigating the connection between symmetries and KPZ scaling in fermionic systems. Additionally, the Hubbard model is integrable [39], which further adds to its appeal for such studies. The existence of two non-abelian symmetries in the model enables us to explore the conjecture in both the spin and charge sectors, thus providing us with a greater flexibility in examining the role of non-abelian symmetries.

We tackle the problem from two distinct setups. First, we study a quench protocol within a closed Hubbard chain by time evolving the density matrix $\rho(t)$. We consider a mixed initial state, asymptotically close to the infinite temperature ($T = \infty$) state, with a weak imbalance either in the occupation (charge density) or the magnetization across an interface in the middle of the chain. Within this setup, we determine the universal functions for the charge and magnetization gradients, as well as the charge and spin currents. Second, we examine an open system setup, where the Hubbard chain is locally coupled to external markovian reservoirs at both ends, and investigate how the charge current scales with system size in the non-equilibrium steady state (NESS). Our results clearly corroborate the KPZ scaling conjecture. With respect to the first setup, our results are consistent with those of Ref. [37], while they represent an improvement with respect to convergence as well as extension to the regimes of partially broken non-abelian symmetries, i.e. considering initial states with non-half filling or non-zero magnetization, as well as offer some quantitative studies of crossover regimes. With respect to the second setup, our results are again consistent with KPZ scaling [10], while they are not consistent with the previous boundary driven Lindblad study of the Hubbard chain [36]. Our detailed study of convergence to NESS reported below shows that previous results [36] were not yet fully converged and hence displayed an illusion of Ohm's law behavior.

The structure of our paper is as follows: In Sec. II, we provide an introduction to the Hubbard model and discuss its non-abelian symmetries. In Sec. III, we describe the quench protocol used to investigate the KPZ scaling. In Sec. IV, we present the results for the non-interacting limit where transport is ballistic. Moving on to the finite U case, Sec. V presents scaling results for the average occupation, average magnetization, and associated currents in the context of KPZ scaling. However, as we move away from half-filling in Sec. VI, we show that the KPZ scaling is lost in the charge sector, and the system displays ballistic transport. In Sec. VII, we study the scaling of the NESS current in an open setup with respect to the system size. We show that it displays a superdiffusive behavior, thus corroborating the results obtained in the quench setup. Finally, in Sec. VIII, we summarize our findings and present our conclusions.

II. HUBBARD MODEL, SYMMETRIES AND INTEGRABILITY

The Hubbard model is a simplified model of the behavior of interacting fermions on a lattice, and has proven to be a valuable tool in understanding the properties of strongly correlated electron systems. The Hamiltonian of the one-dimensional (1D) Hubbard chain on L sites reads

$$H = -\frac{J}{2} \sum_{\sigma} \sum_{x=-L/2}^{L/2-2} (c_{x\sigma}^{\dagger} c_{x+1\sigma} + h.c.) + \frac{U}{2} \sum_x (n_x - 1)^2 \quad (1)$$

where $c_{x\sigma}^{(\dagger)}$ denote the annihilation (creation) operators of a fermion at site x on the chain, with spin σ , and $n_x = \sum_{\sigma} c_{x\sigma}^{\dagger} c_{x\sigma}$ denotes the occupation number operator. The first term in the Hamiltonian describes the kinetic energy of the fermions, as they can hop between neighboring sites with amplitude J . The second term represents the Coulomb repulsion between fermions on the same site, where U is the strength of the interaction. In our calculations we consider the energy units of J and measure time in units of $1/J$, i.e. $J \equiv 1$. In the Hubbard model, the local Hilbert space that refers to the set of possible states at a single lattice site has dimension $d = 4$, and is spanned by the empty state, the two possible spin states of a fermion of spin $S = 1/2$, and the doubly-occupied state. Thus, the basis states of the local Hilbert space are denoted as $\{|0\rangle, |\downarrow\rangle, |\uparrow\rangle, |\uparrow\downarrow\rangle\}$.

The Hubbard model has several symmetries that are important for understanding its behavior [40]. It exhibits an $SU_s(2)$ spin symmetry which arises from the total spin conservation, i.e., each component of

$$\mathbf{S} = \frac{1}{2} \sum_{x,\sigma\sigma'} c_{x\sigma}^{\dagger} \boldsymbol{\sigma}_{\sigma\sigma'} c_{x\sigma'}, \quad (2)$$

commutes with the Hamiltonian (1). This symmetry is broken in the presence of an external magnetic field, or in the presence of a spin imbalance within the chain ($\langle n_{\uparrow} \rangle \neq \langle n_{\downarrow} \rangle$).

The Hubbard model displays also a $U_c(1)$ charge symmetry, that arises from the conservation of the total number of electrons in the system,

$$N = \sum_{x,\sigma} c_{x\sigma}^{\dagger} c_{x\sigma}. \quad (3)$$

At half-filling, $\langle n \rangle = 1$ (i.e., $N = L$), the $U_c(1)$ symmetry is raised to a non-abelian $SU_c(2)$ symmetry, sometimes referred to as ' η -pairing' [41]. The operators η^{\dagger} and η , defined as

$$\eta^{\dagger} = \sum_x (-1)^x c_{x\uparrow}^{\dagger} c_{x\downarrow}^{\dagger}, \quad \eta = \sum_x (-1)^x c_{x\downarrow} c_{x\uparrow}, \quad (4)$$

together with the appropriately shifted particle number operator, $\eta_z \equiv N - L$, satisfy the $SU(2)$ algebra, and

commute with the Hamiltonian of the half filled Hubbard model (1), proving its $SU_c(2)$ symmetry,

$$\begin{aligned} [H, \eta^\dagger] &= 0 & [H, \eta] &= 0 & [H, \eta_z] &= 0 \\ [\eta_z, \eta^\dagger] &= \eta^\dagger & [\eta_z, \eta] &= -\eta & [\eta^\dagger, \eta] &= 2\eta_z. \end{aligned} \quad (5)$$

The square of the total pseudo-charge operator is

$$\boldsymbol{\eta}^2 = \frac{1}{2}(\eta^\dagger \eta + \eta \eta^\dagger) + \eta_z^2, \quad (6)$$

and it also commutes with the Hamiltonian (1).

Time evolution with H thus respects $SU_c(2) \times SU_s(2)$ symmetry. While the infinite temperature state also obeys these symmetries, more complex initial states can, however, break them. At the $SU_c(2)$ symmetric point the 4-dimensional local Hilbert space can be organized into two-dimensional charge-spin multiplets, $\{|\uparrow\rangle, |\downarrow\rangle\}$ and $\{|\uparrow\downarrow\rangle, |0\rangle\}$. Away from half filling, the second multiplet breaks into two one-dimensional states that are distinguished by their $U_c(1)$ charge [42]. Similarly, creating a spin imbalance in the initial state breaks the $SU_s(2)$ symmetry. In the limit of very small symmetry breaking, however, linear response is still governed by the unperturbed, $SU_s(2) \times SU_c(2)$ symmetrical system.

In addition to continuous symmetries, the Hubbard model with nearest-neighbor hopping displays also other, discrete symmetries such as the particle-hole (p-h) [43] or the duality symmetry [44, 45], but in our analysis, only the continuous abelian and non-abelian symmetries are relevant, discrete symmetries have just been mentioned for the sake of completeness.

In addition to the global symmetries discussed above, the one-dimensional Hubbard model possesses an infinite number of conservation laws [39], and is exactly solvable by Bethe-Ansatz [46–48]. Therefore, it is an excellent candidate to explore the link between KPZ scaling, integrability and global non-abelian symmetries.

III. QUENCH PROTOCOL

In the following, we present the scenario in which the initial state is prepared with an imbalance, either in the occupation or the magnetization. In the infinite temperature state, the thermal energy of the particles is so high that there is no correlation or coherence among the particles. Therefore, the $T = \infty$ state is described by the diagonal density matrix

$$\rho(T = \infty) = 4^{-L} \prod_x \mathbb{1}_x \quad (7)$$

in which all local states are equally populated, i.e.,

$$\mathbb{1}_x = |0\rangle\langle 0| + |\uparrow\rangle\langle \uparrow| + |\downarrow\rangle\langle \downarrow| + |\uparrow\downarrow\rangle\langle \uparrow\downarrow|. \quad (8)$$

We consider a quench protocol in which the system is prepared in an inhomogeneous state, corresponding to a

small deviation from the homogeneous $T = \infty$ state such that the initial state consists of two halves with a charge imbalance,

$$\rho(t=0) = \prod_{x=-L/2}^{L/2} \rho_x(0) \quad (9)$$

with

$$\rho_x(0) = \begin{cases} \frac{1}{4}\mathbb{1}_x - \frac{\mu}{2}|0\rangle\langle 0| + \frac{\mu}{2}|\uparrow\downarrow\rangle\langle \uparrow\downarrow|, & x < 0 \\ \frac{1}{4}\mathbb{1}_x - \frac{\mu}{2}|0\rangle\langle 0| - \frac{\mu}{2}|\uparrow\downarrow\rangle\langle \uparrow\downarrow|, & x \geq 0 \end{cases}, \quad (10)$$

where $\mu \ll 1$ is a parameter that controls the deviation from the $T = \infty$ state, that corresponds to $\mu = 0$. The average occupation at any time t can be expressed in terms of the density matrix as

$$\langle n_x \rangle(t) = \text{tr}\{\rho(t) c_{x\sigma}^\dagger c_{x\sigma}\} \quad (11)$$

and evaluates at $t = 0$ to

$$\langle n_x \rangle(t=0) = \begin{cases} 1 + \frac{\mu}{2}, & x < 0 \\ 1 - \frac{\mu}{2}, & x \geq 0 \end{cases} \quad (12)$$

At $t = 0$, the density profile corresponds to a step function with a small imbalance in the occupations $\propto \mu$ between the two halves of the chain. Notice that this initial state breaks the $SU_c(2)$ symmetry, but still preserves the spin $SU_s(2)$ symmetry.

As the initial state does not commute with the Hamiltonian (1), the system is out of equilibrium, and undergoes non-trivial dynamics. Numerically, we solve the von-Neuman equation that governs the evolution of the system's density matrix

$$i\frac{\partial}{\partial t}\rho(t) = [H, \rho(t)], \quad (13)$$

We solve Eq. (13) by using the vectorization procedure [49–51] $\rho(t) \rightarrow |\rho\rangle$ within the matrix product state framework [42, 52, 53]. For that, we use the superfermion representation [50, 54, 55] which introduces a new set of annihilation (creation) operators $\tilde{c}_{x,\sigma}^{(\dagger)}$ that satisfy the usual anticommuting relations, and generate the dual Fock space [50].

To obtain the time evolution of $|\rho(t)\rangle$, we utilized the time-evolving block decimation [53, 56–59], with abelian symmetry operators, $U_c(1) \rightarrow \mathbb{U}_c(1)$ and $U_s(1) \rightarrow \mathbb{U}_s(1)$ extended to the vectorized Liouville space [42]. In addition, we also solve the problem analytically for the non-interacting system ($U = 0$) to benchmark our TEBD computations.

Unlike usual TEBD simulations, which break down after relatively short times, here we can use TEBD simulations with a small maximum bond dimension up to rather long times and for relatively large system sizes due to the slow growth of operator entanglement (en-

tanglement of vectorized density matrix) [12]. This is probably a consequence of having initial states close to the $T = \infty$ state. Computational time is further reduced by exploiting abelian charge and spin symmetries in the calculations. If not otherwise specified, results presented in this work have been obtained by using a bond dimension for the multiplets $M = 100$, which guarantees an error of $\varepsilon < 10^{-7}$ in the discarded Schmidt coefficients. Further details on the actual numerical method have been presented in Ref. [42].

An analogous quench protocol can be implemented in the spin sector, which, in particular at half-filling, allows to test the spin-charge duality. For that, we impose a weak imbalance in the magnetization at $t = 0$. The initial density matrix is given by (9) with the local density matrices $\rho_x(0)$ given by

$$\rho_x(0) = \begin{cases} \frac{1}{4} \mathbb{1}_x + \frac{\mu_z}{2} |\uparrow\rangle\langle\uparrow| - \frac{\mu_z}{2} |\downarrow\rangle\langle\downarrow|, & x < 0 \\ \frac{1}{4} \mathbb{1}_x - \frac{\mu_z}{2} |\uparrow\rangle\langle\uparrow| + \frac{\mu_z}{2} |\downarrow\rangle\langle\downarrow|, & x \geq 0 \end{cases}, \quad (14)$$

where μ_z controls spin polarization on the two halves of the chain, $\delta s_z(x, 0) = \langle \frac{1}{2} \sigma^z(x, t) \rangle_{t=0} = \pm \mu_z/2$ for $x < 0$ and $x \geq 0$, respectively.

IV. BALLISTIC BEHAVIOR ($U = 0$)

In the non-interacting limit, $U = 0$, the quasiparticles move independently and are not scattered by each other. Their dispersion relation is given by the usual tight-binding formula, $\varepsilon_k = -J \cos(k)$, which determines their maximal quasiparticle velocity, $v_{\max} = J = 1$, identified as the Lieb-Robinson velocity [60, 61]. In the absence of interactions, quasiparticles motion is coherent, and transport is referred to as 'ballistic', implying a linear relation between distance and traveling time. While in this section we present results specific to charge transport at half filling, it is important to remark that for $U = 0$ ballistic transport persists for any filling, both in the charge and in the spin sector.

In Fig. 1 we display the evolution of the average occupation $\delta n(x, t) = \langle n(x) \rangle(t) - \langle n \rangle$ and the particle current

$$j(x, t) = \text{tr} \left\{ \frac{i}{2} [c_{x+1, \sigma}^\dagger c_{x\sigma} - c_{x\sigma}^\dagger c_{x+1\sigma}] \rho(t) \right\}, \quad (15)$$

along the chain after the initial quench. These both display light-cone propagation of quasiparticles with a constant velocity, v_{\max} . To confirm ballistic transport, we performed quantitative analysis of charge and current equilibration, and the scaling of charge and current profiles. Fig. 2 demonstrates ballistic scaling for $U = 0$: the rescaled profiles for $\delta n(x, t)$ and $j(x, t)$ collapse onto a single universal curve, when plotted against x/t . The total number of particles transferred across the interface is another useful quantity, whose asymptotic behavior in the long time limit allows to identify the type of dynamics [9, 19]. The total charge across the interface scales

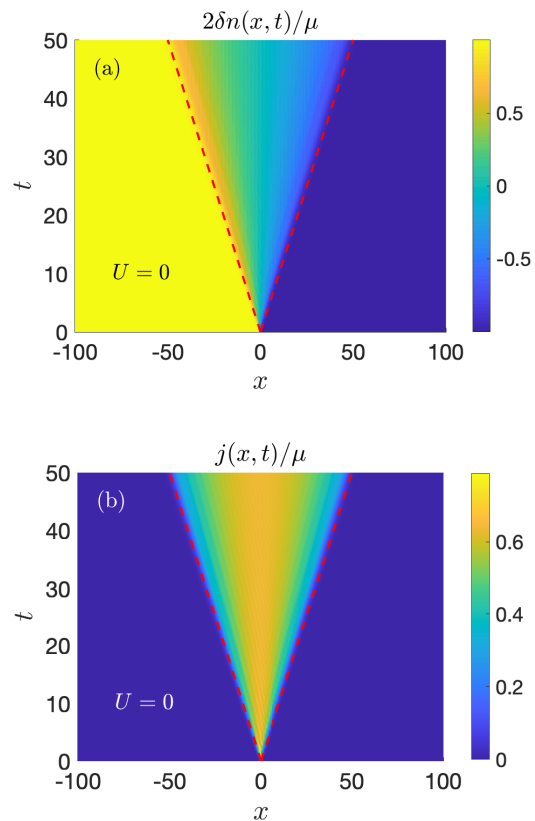


FIG. 1. Heatmap of occupation density and charge current in the non-interacting case $U = 0$. (a) Time evolution of the average occupation along the chain with respect to half filling $\delta n(x, t) = \langle n(x, t) \rangle - \langle n \rangle$, with $\langle n \rangle = 1$. (b) Average current along the chain, demonstrating a regular light cone propagating ballistically with a constant Lieb-Robinson velocity of $v_F \approx J$. The red dashed lines provide a visual guide, corresponding to $t = x/v_F$. The system size is fixed at $L = 200$ sites.

as

$$N_{\text{tr}}(t) = \int_0^t j(0, t') dt' \propto t^\alpha, \quad (16)$$

with an exponent $\alpha = 1/z$. For ballistic transport, one has $\alpha = 1$, while diffusive transport is characterized by $\alpha = 1/2$, and anomalous diffusion by an exponent different from these. As Fig. 3 shows, $j(0, t)$ exhibits a rich structure. Following the quench, the current displays transient oscillations with an approximate frequency $\omega \approx \omega_J \equiv J$, and an amplitude decaying as $\propto t^{-1}$. In the long-time limit, the current approaches a finite asymptotic value. The inset displays the total number of particles transferred across the interface, increasing linearly with time, $N_{\text{tr}}(t) \propto t$, corresponding to ballistic transport.

Our TEBD results are consistent with the analytical findings. By assuming periodic boundary conditions (PBC) and performing a Fourier transform of the time

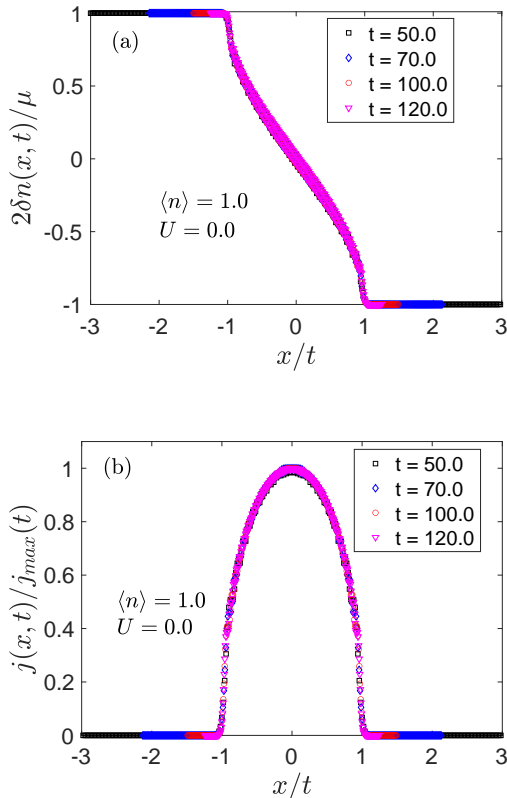


FIG. 2. (a) Rescaled profiles for the average occupation $\delta n(x, t)$ at $U = 0$ and half filling at various times, plotted as a function of x/t to display the universal ballistic scaling. (b) The corresponding current profile, $j(x, t)$ exhibits a similar ballistic scaling.

evolution, it is possible to express the time dependence of the annihilation (creation) operators in the Heisenberg picture in terms of Bessel functions of the first kind,

$$c_{\bar{x}\sigma}(t) = \sum_x i^{x-\bar{x}} J_{x-1}(\omega_J t) c_{\bar{x},\sigma}, \quad (17)$$

with the frequency associated with the hopping integral, $\omega_J = J$.

By solving the von Neumann equation (13) for the density matrix $\rho(t)$, we can determine the expectation value of the current operator at site x along the chain. Using the standard approach of calculating the trace of the product of the density matrix and the current operator, Eq. (15), we obtain the current at the interface $x = 0$ at any later time,

$$j(0, t) = \mu \sum_{x=-L/2}^{L/2-1} \sum_{\sigma} J_x(\omega_J t) J_{x+1}(\omega_J t). \quad (18)$$

This result matches with the TEBD data, as shown in

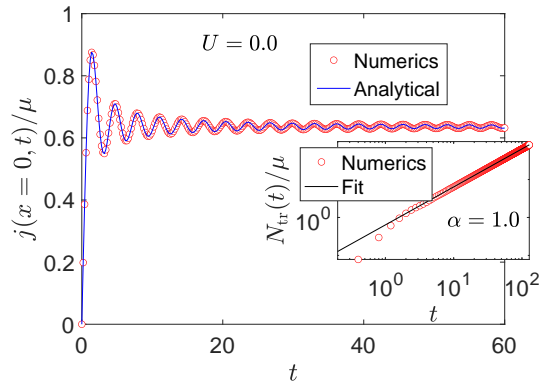


FIG. 3. Time evolution of the current $j(x = 0, t)$ across the interface at $U = 0$. The symbols correspond to the numerical results obtained using TEBD, while the solid line represents the analytical expression (18). The transient oscillations decay as $\propto t^{-1}$, and the current remains constant in the limit of $t \rightarrow \infty$, indicating a ballistic behavior. The inset shows the total number of particles that tunnel across the interface $N_{tr}(t)$ together with the power law fitting, which indicates a scaling exponent $\alpha \approx 1$ associated with ballistic transport.

the main panel of Fig. 3.

V. SUPERDIFFUSIVE BEHAVIOR AT HALF-FILLING ($U \neq 0$, $\langle n \rangle = 1$)

In general, superdiffusive behavior refers to a diffusion process in which the mean square displacement of quasi-particles increases faster than linear with time, but slower than quadratic. This behavior is often characterized by an asymptotic power-law relationship

$$\langle \Delta x^2 \rangle \approx 2D t^{2\alpha}, \quad (19)$$

with an exponent α greater than $1/2$ and smaller than 1 , and D , the anomalous diffusion constant. In the specific case of the KPZ scaling, the superdiffusive exponent is $\alpha_{sd} = 2/3$.

In this section, we study transport in the presence of interactions at half filling, $\langle n \rangle = 1$, and demonstrate superdiffusive behavior. At half-filling, pseudo-charge and spin $SU(2)$ symmetries are related by duality, which implies that spin and charge transport have identical properties.

A. Charge sector

With the initial density matrix $\rho(0)$ as defined in Eq. (9), we assess the transport properties in the charge sector by analyzing the decay of the average density and current

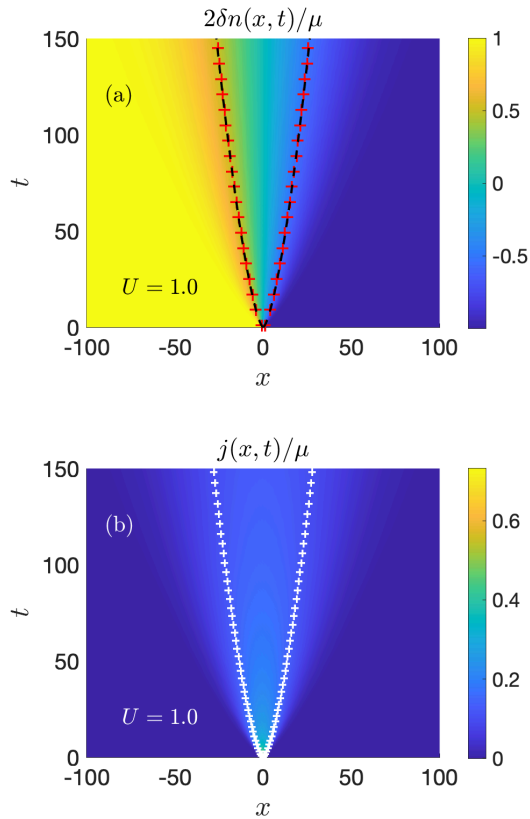


FIG. 4. Spatio-temporal evolution of the average occupation $\delta n(x, t)$ and the average current $\langle j(x, t) \rangle$ along the chain at half-filling with a finite interaction strength $U = 1.0$, indicate a superdiffusive behavior. Symbols correspond to mid-value contours, where $2\delta n(x, t)/\mu = \pm 0.5$, while dashed lines indicate $t^{2/3} = rx/v_F$, with a scaling factor $r = 1.1$.

profiles. In Fig. 4 we display the spatio-temporal evolution of $\delta n(x, t)$ and the average current, $j(x, t)$, which both indicate slower than ballistic propagation of the quasiparticles.

Indeed, the density and the current density profiles can be both presented as a function of a single scaling variable, x/t^α , and collapse onto a single curve at large times, with $\alpha_{sd} = 2/3$, as predicted by KPZ scaling. This is illustrated in Fig. 5(a,b), where $\delta n(x, t)$ and $j(x, t)$ are plotted against x/t^α for $U = 1$, and shown to exhibit clear superdiffusive scaling with $\alpha = 2/3$.

These results are corroborated with Fig. 6, showing the power law decay of the current across the interface in the long time limit, $j(0, t) \sim t^{\alpha-1} = t^{-1/3}$, implying that the total number of particles transferred across the interface scales as, $N_{tr}(t) \sim t^\alpha = t^{2/3}$ (see inset).

The current j and density gradient $\partial_x n$ exhibit similar, universal profiles [9]. The density profile, in particular, exhibits a scaling,

$$\delta n(x, t) = \mu \rho(bx/t^\alpha) \quad (20)$$

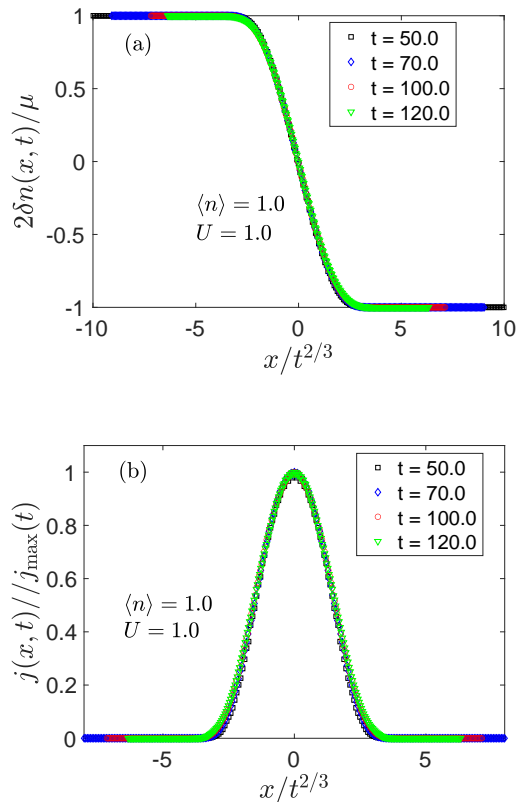


FIG. 5. Rescaled profiles of (a) the average occupation $\delta n(x, t)$, and (b) the current $j(x, t)$, at half filling for $U = 1.0$ at various times. Both display universal superdiffusive scaling, in terms of $x/t^{2/3}$.

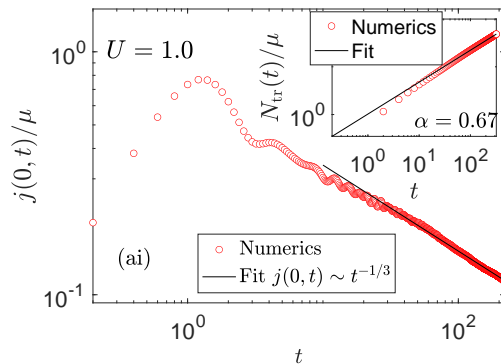


FIG. 6. The time dependence of the current across the interface follows a power-law decay, $\sim t^{1-\alpha}$ with a superdiffusion exponent, $\alpha_{sd} \approx 2/3$. The transferred charge scales as $N_{tr}(t) \sim t^\alpha = t^{2/3}$, as shown in the inset. System size is $L = 300$ sites.

with $\rho(y)$ a scaling function satisfying $\rho(\mp\infty) = \pm 1/2$,

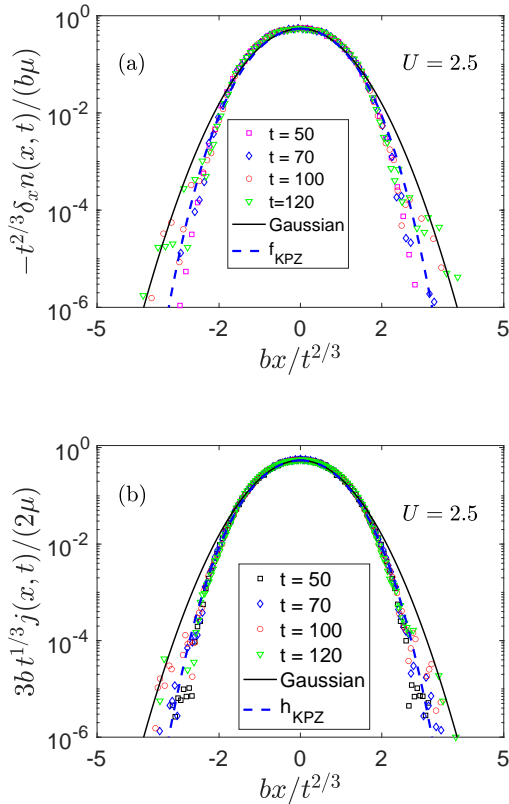


FIG. 7. The density gradient $\delta_x n(x, t) = \delta n(x, t) - \delta n(x - 1, t)$ (panel a), as well as the current density $j(x, t)$ (panel b) display universal KPZ scaling. Here f_{KPZ} is the KPZ scaling function [20], while h_{KPZ} has been computed by integrating Eq. (23). Notice that a single scaling parameter $b = 0.98$ is used to fit all profiles simultaneously on both panels.

and the scaling factor, b , related to the diffusion constant, $b \sim 1/\sqrt{D}$. This immediately leads to the density gradient scaling as,

$$\partial_x n(x, t) = -\frac{b\mu}{t^\alpha} f(bx/t^\alpha), \quad (21)$$

with the scaling function $f(y) = -\rho'(y)$. Notice that $f(y)$ obeys the sum rule, $\int dy f(y) = 1$.

The scaling form of the current follows from the continuity equation, $\dot{n}(x, t) + \partial_x j(x, t) = 0$, implying

$$j(x, t) = \frac{\mu}{b} \alpha t^{\alpha-1} h(bx/t^\alpha), \quad (22)$$

with the scaling function $h(y)$ related to $f(y)$ by the differential equation,

$$h'(y) = -y f(y). \quad (23)$$

As shown in Fig. 7, $j(x, t)$ and $\partial_x n(x, t)$ indeed satisfy the scaling forms, (22) and (21). We emphasize that

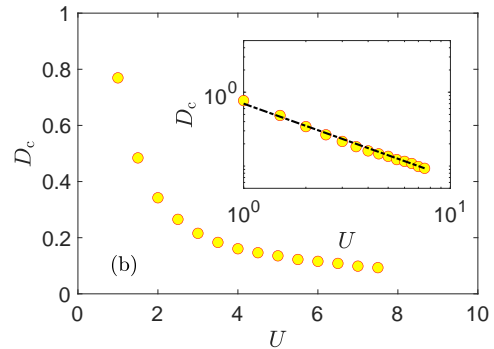


FIG. 8. Charge diffusion coefficient D_c as a function of the interaction strength U . This relationship is shown in the main plot, while the inset displays the same data on a logarithmic scale. The dashed line in the inset corresponds to a behavior proportional to $D_c \sim 1/U$.

these scaling forms are just simple consequences of the rather natural scaling ansatz, (20) and the conservation of electron charge.

We remark that in case of a Gaussian current profile, $h(y) \sim e^{-\kappa y^2/2}$, $h(y)$ and $f(y)$ assume the same, Gaussian forms (apart from a prefactor). However, this relation is violated for any other profile, including the KPZ profile discussed here.

To establish the system's universal dynamics conclusively, we now compare the scaling functions $f(y)$ and $h(y)$ to the KPZ scaling function. For small μ , one can use linear response theory to prove that the equilibrium correlation function, $\chi_n(x, t) \equiv \langle n(x, t)n(0, 0) \rangle$, and the gradient $\partial_x n(x, t)$ are proportional to each other [9],

$$\chi_n(x, t) = -\lim_{\mu \rightarrow 0} \frac{1}{\mu} \partial_x \langle n(x, t) \rangle \approx -\frac{1}{\mu} \partial_x n(x, t) \quad (24)$$

where $\delta_x n(x, t) = \langle n(x, t) \rangle - \langle n(x - 1, t) \rangle$ stands for the finite difference of the density.

The gradient profile in our set-up is therefore just the density-density correlation function [9], which is well documented in the KPZ model. The numerically obtained density gradient and current profile scaling functions are displayed in Figs. 7 (a,b), together with the tabulated KPZ (f_{KPZ}) and simple gaussian scaling functions [20], and h_{KPZ} computed from Eq. (23). Our numerical results show that the KPZ scaling functions accurately describe both the density gradient and the average current profiles, while the Gaussian scaling function does not. These results, together with the scaling properties of charge transfer and the deformation of the light cone, establish KPZ scaling of the charge correlations in the half-filled infinite temperature state.

Let us close this section by discussing the interaction dependence of the anomalous diffusion constant. Classi-

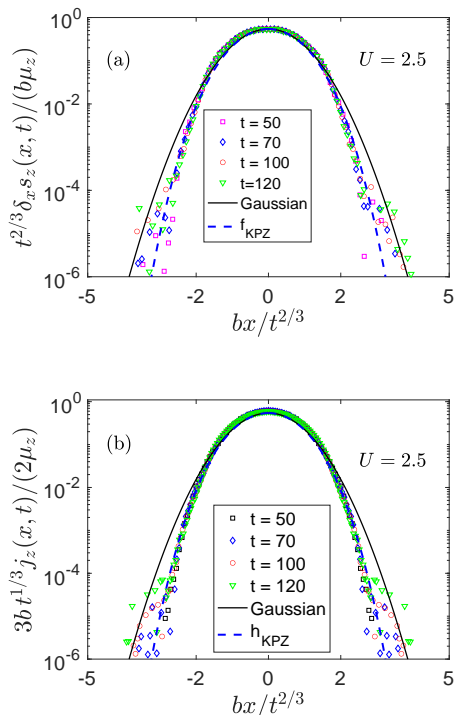


FIG. 9. The magnetization gradient, $\delta_x s_z(x, t) = \delta s_z(x, t) - \delta s_z(x-1, t)$ (panel a), and the spin current density $j_z(x, t)$ (panel b) display also universal KPZ scaling at half filling. We use $b = 0.98$ on both panels.

cally, the correlation function, $\chi_n(x, t) \equiv \langle n(x, t)n(0, 0) \rangle$, is just the probability that a particle originally at $x = 0$ reaches position x at time t ,

$$P(x, t|0, 0) = \chi_n(x, t). \quad (25)$$

The scaling form of the gradient, (21) therefore implies,

$$P(x, t|0, 0) = \frac{b}{t^\alpha} f(bx/t^\alpha). \quad (26)$$

We can then express the variance of the distance as

$$\langle x^2 \rangle = \int dx x^2 P(x, t|0, 0) = 2 D_c t^{2\alpha}, \quad (27)$$

with the charge diffusion constant expressed as

$$D_c = \mathcal{I}/b^2, \quad (28)$$

with $\mathcal{I} = \frac{1}{2} \int dy y^2 f_{\text{KPZ}}(y) = 0.25$ for the KPZ scaling function.

We can thus determine the anomalous diffusion constant (in units of $a^2 J^{2\alpha}$) by extracting the scaling factor b from the current or density gradient profiles, and using the relation, $D = \mathcal{I}/b^2$. Alternatively, we can compute $\langle x^2 \rangle$ by using the profile, $\delta_x n(x, t)$ as a probability distribution,

and divide it by $t^{4/3}$. Both methods yield the same values for D within numerical precision.

The interaction dependence of D is displayed in Fig. 8. Although we cannot assess the precise U dependence of D_c at small interactions, at moderate interactions we find a scaling $D_c \sim U^{-1}$, which may be related to the reduction of the hopping amplitude of doublons to neighboring empty sites, $\sim J^2/U$.

B. Spin sector

We also analyzed the scaling of the magnetization profile and that of the spin current density close to the interface, and extracted the corresponding scaling functions. All our findings support the notion of charge-spin duality at the $SU_c(2) \otimes SU_s(2)$ point. For example, in Fig. 9, we show the scaling functions corresponding to the magnetization gradient, $\delta_x s_z(x, t)$, and the spin current $j_z(x, t)$. These obey the scaling equations, Eqs. (21) and (22), but with $\delta_x n(x, t)$ and $j(x, t)$ replaced by $\delta_x s_z(x, t)$ and $j_z(x, t)$, respectively.

C. Scaling exponents and finite size effects

Our findings indicate quite clearly the presence of KPZ scaling. However, obtaining the scaling exponent accurately requires sufficiently large system sizes and a long enough evolution times. To avoid spurious effects like reflection at the boundaries, the simulations' time span must be restricted by the actual size of the system, $t \lesssim 2L$.

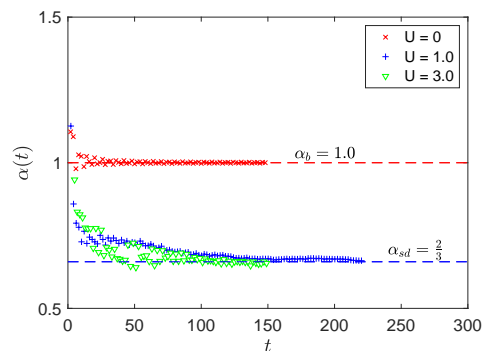


FIG. 10. Scaling exponents obtained from the logarithmic differential of the charge transferred across the interface. At $U = 0$, the exponents approach the ballistic value, $\alpha_b = 1.0$ already at relatively short times. At $U \neq 0$, the exponent converges to the asymptotic superdiffusive value, $\alpha_{\text{sd}} = \frac{2}{3}$. For intermediate interactions (e.g., $U = 1$), the convergence is slow and the asymptotic value is approached only on time scales $t \approx 200$, which requires large system sizes (up to $L \approx 400$ sites). For stronger interactions ($U \geq 3$) the convergence is faster, and happens on time scales $t \lesssim 100$.

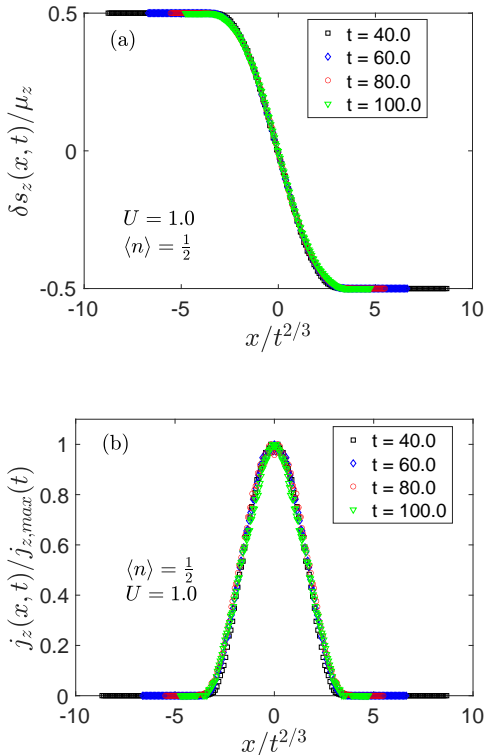


FIG. 11. The rescaled profiles of (a) the average magnetization $\delta s_z(x, t)$ at a quarter filling, where $\langle n \rangle = 1/2$, and (b) the average spin current $j_z(x, t)$ along the chain, both exhibiting $x/t^{2/3}$ scaling.

Additionally, the strength of the interaction is a crucial factor to consider. Fig. 10 displays the exponent $\alpha = 1/z$ obtained from the logarithmic differential of the total charge across the interface,

$$N_{\text{tr}}(t) \sim t^\alpha. \quad (29)$$

In the ballistic case, $U = 0$, the convergence to the asymptotic values occurs rapidly, and relatively small system sizes are sufficient for accurate calculations. On the other hand, for $U \neq 0$, convergence depends crucially on the interaction strength; for stronger interactions the logarithmic differential converges faster, although it becomes more noisy, while for small interactions convergence is very slow. Even for intermediate values, $U \sim 1$, time scales of different processes overlap, and obtaining the correct exponent requires simulations of very long duration and, correspondingly, large enough system sizes. Although we cannot reach convergence for $d \ln(N_{\text{tr}}(t)) / d \ln t$ in the small coupling regime $U \lesssim 1$, the tendency observed at intermediate couplings brings us to conclude that at sufficiently long times a *superdiffusive* behavior emerges at any finite coupling, U . As we shall see, sufficiently large system sizes and a very careful analysis is needed

also the open system setup, to investigate the asymptotic behavior.

VI. AWAY FROM HALF-FILLING ($U \neq 0$, $\langle n \rangle \neq 1$)

Away from half-filling, the $SU_c(2)$ pseudo-charge symmetry is reduced to a $U_c(1)$ symmetry. This implies that the density matrix $\rho(t)$ is no longer invariant under rotations generated by $\boldsymbol{\eta}$. On the other hand, the model still retains its spin $SU_s(2)$ symmetry. We are thus able to investigate the conjecture that links non-abelian symmetries and the KPZ scaling in the spin sector, even when the $SU_c(2)$ symmetry is broken.

In the following, we present data both in the spin and in the charge sectors, obtained at quarter filling, $\langle n \rangle = 1/2$. Fig. 11 shows the scaling behavior of the magnetization and spin current profiles, along with the corresponding scaling function. Only a scaling with $x/t^{2/3}$ results in a proper data collapse for both $\delta s_z(x, t)$ and $j_z(x, t)$, and the universal curve displayed in Fig. 12 demonstrates a distinct KPZ dependence.

In contrast, quasi-particles move ballistically in the charge sector. The average occupation $\delta n(x, t)$, e.g., presented in Fig. 13 displays a typical light cone pattern. Interestingly, the occupation profile shows two distinct velocities: one that corresponds to the maximum possible velocity of the free particles, i.e., $v_{\max} = J$, and another, smaller velocity that depends on the strength of the interaction U . These findings are consistent with similar observations in the context of GHD, where multiple light velocities are also observed in some cases [62–64]. Figs. 14.a and b show the spatial charge and charge current profiles at various times and demonstrate that only a ballistic rescaling, $\sim x/t$, result in the proper data collapse for both the occupation and the charge current, and also the clear development of the two fronts.

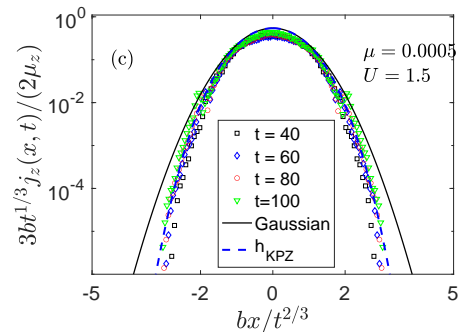


FIG. 12. The scaling function for the spin current along with the corresponding KPZ scaling function at quarter filling $\langle n \rangle = 1/2$ and $U = 1.5$. The parameter b is fixed to $b = 0.75$.

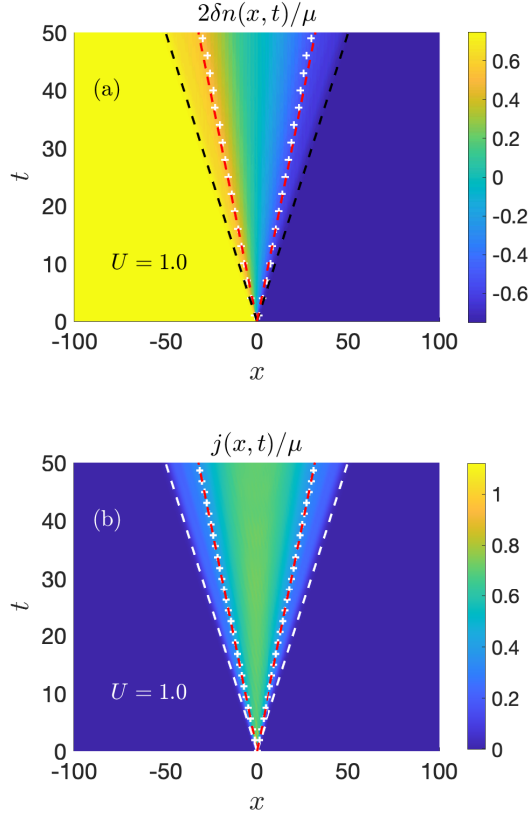


FIG. 13. Time evolution of the average occupation and average charge current along the chain at quarter filling for $U = 1.0$. Two fronts moving at different velocities are clearly visible.

VII. HUBBARD CHAIN COUPLED TO TWO RESERVOIRS

So far we have investigated KPZ scaling in terms of a quench protocol. We now turn to a different setup, and explore the emergence of the KPZ scaling in a Hubbard chain coupled to external markovian (Lindbladian) reservoirs, generating local particle gain and loss at both ends. We investigate the dynamics and various observables, such as the average occupation along the chain and the average current in the non-equilibrium steady state (NESS).

We perform TEBD calculations [57, 58] by starting from an infinite temperature state, and solving the Lindblad equation

$$i\dot{\rho} = \mathcal{L}[\rho] = [H, \rho] + i\mathcal{D}[\rho] \quad (30)$$

in the Gorini, Kossakowski, Sudarshan [65] and Lindblad approach [66]. Here H is the Hamiltonian introduced in Eq. (1), while the dissipator term $\mathcal{D}[\rho] = \sum_F \Gamma_F \mathcal{D}_F[\rho]$

$$\mathcal{D}_F[\rho] = 2F\rho F^\dagger - \{F^\dagger F, \rho\} \quad (31)$$

is given in term of the boundary jump operators $F \in$

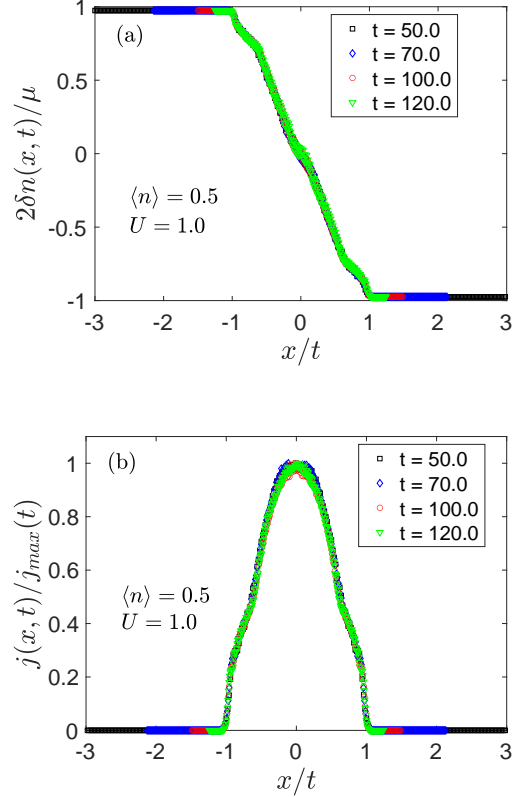


FIG. 14. The rescaled profiles for the average occupation (a) and current (b) at quarter filling for $U = 1$ display ballistic scaling.

$\{c_{-L/2\sigma}, c_{-L/2\sigma}^\dagger, c_{L/2\sigma}, c_{L/2\sigma}^\dagger\}$, acting at the first and last sites of the chain.

To induce a non-equilibrium steady state (NESS) along the chain, we introduce a slight imbalance in the couplings for loss and gain processes at the two ends of the chain. Specifically, on the left the strength for the loss process, $\Gamma_{-L/2,\sigma}^{(-)} = \Gamma(1 - \mu)$ is less than that of the gain process, $\Gamma_{-L/2,\sigma}^{(+)} = \Gamma(1 + \mu)$ for $\mu > 0$, while on the right, loss processes are increased and gain processes reduced, $\Gamma_{L/2,\sigma}^{(\pm)} = \Gamma_{-L/2,\sigma}^{(\mp)}$. Here Γ controls the strength of the coupling to the reservoirs, while the imbalance $\mu \ll 1$ plays the role of an external chemical potential that drives the system toward a NESS.

We used the NA-TEBD approach of Ref. [42] to integrate the Lindblad equation (30). We also verified that the resulting NESS is unique and independent of the initial conditions. Using the infinite temperature state as the initial state, however, allows us to reach NESS more quickly. We presume that NESS is reached once the average current $j(x, t)$ no longer depends on the position x and time. Fig. 15 shows the evolution of the current at several bond positions along the chain, indicating that

stronger interactions lead to slower dynamics and a slower convergence towards NESS.

To capture the KPZ scaling accurately, it is necessary to evolve the system for sufficiently long times, $t \approx 10L/v_F$, such that the system reaches its non-equilibrium steady state. Figure 16 presents the combined finite size and time dependence of the current at the center, $j(x=0, t)$. At short times, the current scales in a diffusive manner, $j(0, t) \sim 1/L$ [36], but displays a superdiffusive scaling, $j(0, t) \sim 1/\sqrt{L}$, once simulation times are long enough.

Fig. 17 depicts a typical occupation profile along the chain in the NESS. At $U = 0$, the average occupation is approximately 1, except for the first and last sites, which exhibit a jump. We have validated these $U = 0$ TEBD results against the 3rd quantization approach [67] (not shown). As U increases, the average occupation is no longer uniform along the chain, but there is still a small jump at the boundaries.

Fig. 18 illustrates how the NESS current, j_{NESS} , changes with system size. For $U = 0$, the current remains constant regardless of the system size, $j_{\text{NESS}} \sim 1/L^0$, char-

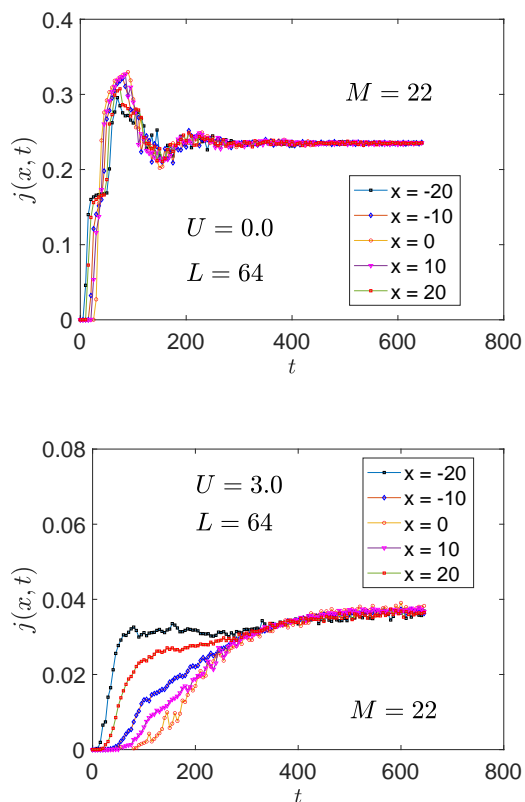


FIG. 15. The evolution of the current as a function of time towards the NESS is shown for different bond positions x along the chain for (a) the non-interacting case ($U = 0$) and (b) $U = 3.0$. The chain length is fixed to $L = 64$ sites. In the interacting regime, the system evolves more slowly towards the NESS.

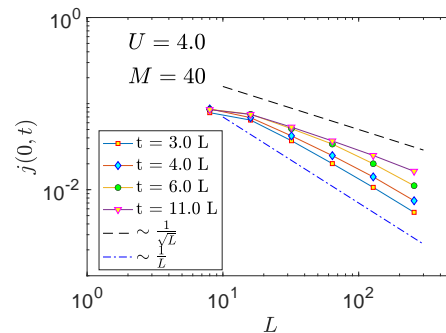


FIG. 16. Scaling of the current as function of the chain length for $U = 4.0$ at different times.

acteristic of ballistic transport. In contrast, for $U \neq 0$, j_{NESS} exhibits a power law dependence on the system size, most consistent with $j_{\text{NESS}} \sim 1/\sqrt{L}$, indicative of superdiffusive transport [10].

In Fig. 18 we also display the bond dimension dependence of the NESS current. Although for small system sizes the slow growth of operator entropy allows us to use small bond dimensions $M \approx 20$, for system sizes exceeding $L > 100$ it is necessary to raise the bond dimension beyond $M > 100$ to obtain reliable results and to capture the scaling exponents accurately, especially for larger values of U .

VIII. CONCLUSIONS

In this work, we have investigated KPZ scaling in the Hubbard model, and explored its connection with non-abelian symmetries. In this regard, the Hubbard model provides an ideal playground, since it is integrable, and at half-filling it possesses two non-abelian symmetries,

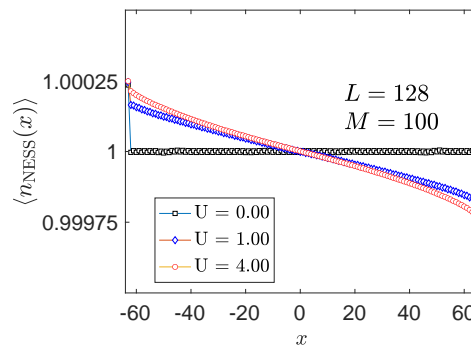


FIG. 17. Average occupation along the chain in the NESS for a chain of length $L = 128$ and different values of U .

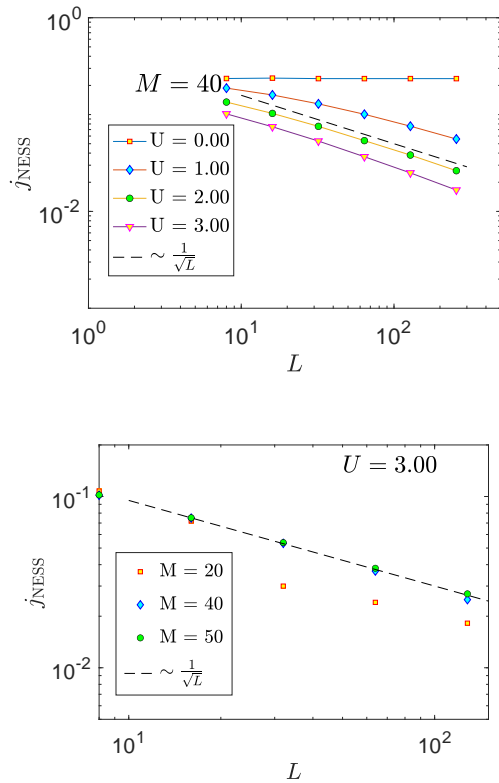


FIG. 18. Top: Interaction and size dependence of j_{NESS} . For $U = 0$, the current is constant, indicating a ballistic behavior, while for finite U $j_{\text{NESS}} \sim \frac{1}{\sqrt{L}}$, confirming KPZ scaling. Bottom: Bond dimension dependence of the steady state current in the middle of the chain as a function of the chain length for $U = 3.0$.

which can both be broken.

For our numerical analysis, we utilized two setups. In the first, 'quench' setup we used a quench protocol, whereby we prepared the system in a mixed state asymptotically close to the $T = \infty$ state, but with weakly imbalanced spatial occupation or magnetization profiles. In the second, 'open' setup we attached particle sources and drains to drive current through the system, and investigated the finite size scaling of the steady state (NESS) current in the linear response regime.

Our calculations confirm that, at half-filling, any small interaction induces KPZ scaling for spin and charge transport: both charge and spin profiles show a distinctive $x/t^{2/3}$ collapse. Our accuracy allowed us to extract the

density-density correlation's function, $\langle n(x, t)n(0) \rangle$ from the data, and confirm that its scaling properties are captured with the universal KPZ scaling function within our numerical accuracy. This scaling analysis also enabled us to extract the anomalous diffusion constant, D and its interaction dependence. The anomalous diffusion is suppressed at large values of U , and D seems to vanish in the $U \rightarrow \infty$ limit. This is somewhat counterintuitive, since, as discussed below, charge transport becomes ballistic once charge $SU_c(2)$ symmetry is broken, and charge fronts can propagate with the Lieb-Robinson velocity, $v_{\text{max}} = aJ$.

As mentioned above, charge transport becomes once we break the charge $SU_c(2)$ symmetry down to $U_c(1)$, by moving away from half-filling. In this case a double front structure appears, associated with two distinct front velocities; the first front propagates with $v_{\text{max}} = aJ$, while the second front lags behind with a smaller, interaction dependent velocity. Spin transport remains, however superdiffusive, as apparently implied by the unbroken $SU_s(2)$ symmetry. The scaling of the NESS current in the open geometry confirmed the superdiffusive scaling as well.

From these calculations it is thus clear that superdiffusive behavior is associated with non-abelian symmetries. Whether integrability is a crucial ingredient, needs to be investigated, though semiclassical results seem to imply that integrability is not essential for the KPZ scaling observed [68].

ACKNOWLEDGMENTS

We thank Örs Legeza for insightful discussions. This research is supported by the National Research, Development and Innovation Office - NKFIH through research grants Nos. K134983 and SNN139581, within the Quantum National Laboratory of Hungary. C.P.M acknowledges support by the Ministry of Research, Innovation and Digitization, CNCS/CCCDI-UEFISCDI, under projects number PN-III-P4-ID-PCE-2020-0277, under the project for funding the excellence, contract No. 29 PFE/30.12.2021. T.P. acknowledges ERC Advanced grant 694544-OMNES and ARRS research program P1-0402. M.A.W has also been supported by the Janos Bolyai Research Scholarship of the Hungarian Academy of Sciences and by the ÚNKP-22-5-BME-330 New National Excellence Program of the Ministry for Culture and Innovation from the source of the National Research, Development and Innovation Fund. We acknowledge KIFÜ for awarding us access to resource based in Hungary.

[1] H. Hinrichsen, Non-equilibrium critical phenomena and phase transitions into absorbing states, *Advances in Physics* **49**, 815 (2000).

[2] G. Ódor, Universality classes in nonequilibrium lattice systems, *Rev. Mod. Phys.* **76**, 663 (2004).

[3] M. Kardar, G. Parisi, and Y.-C. Zhang, Dynamic scaling of growing interfaces, *Phys. Rev. Lett.* **56**, 889 (1986).

- [4] J. Krug, Origins of scale invariance in growth processes, *Advances in Physics* **46**, 139 (1997).
- [5] T. Kriecherbauer and J. Krug, A pedestrian's view on interacting particle systems, kpz universality and random matrices, *Journal of Physics A: Mathematical and Theoretical* **43**, 403001 (2010).
- [6] I. Corwin, The kardar–parisi–zhang equation and universality class, *Random Matrices: Theory and Applications* **01**, 1130001 (2012).
- [7] J. Villain, Continuum models of crystal growth from atomic beams with and without desorption, *J. Phys. I France* **1**, 19 (1991).
- [8] T. Halpin-Healy and Y.-C. Zhang, Kinetic roughening phenomena, stochastic growth, directed polymers and all that. aspects of multidisciplinary statistical mechanics, *Physics Reports* **254**, 215 (1995).
- [9] M. Ljubotina, M. Žnidarič, and T. Prosen, Kardar-parisi-zhang physics in the quantum heisenberg magnet, *Phys. Rev. Lett.* **122**, 210602 (2019).
- [10] M. Žnidarič, Spin transport in a one-dimensional anisotropic heisenberg model, *Phys. Rev. Lett.* **106**, 220601 (2011).
- [11] T. Prosen and B. Žunkovič, Macroscopic diffusive transport in a microscopically integrable hamiltonian system, *Phys. Rev. Lett.* **111**, 040602 (2013).
- [12] M. Ljubotina, M. Žnidarič, and T. Prosen, Spin diffusion from an inhomogeneous quench in an integrable system, *Nature Communications* **8**, 16117 (2017).
- [13] B. Bertini, F. Heidrich-Meisner, C. Karrasch, T. Prosen, R. Steinigeweg, and M. Žnidarič, Finite-temperature transport in one-dimensional quantum lattice models, *Rev. Mod. Phys.* **93**, 025003 (2021).
- [14] A. Das, M. Kulkarni, H. Spohn, and A. Dhar, Kardar-parisi-zhang scaling for an integrable lattice landau-lifshitz spin chain, *Phys. Rev. E* **100**, 042116 (2019).
- [15] v. Krajinik and T. Prosen, Kardar–parisi–zhang physics in integrable rotationally symmetric dynamics on discrete space–time lattice, .
- [16] D. Roy, A. Dhar, H. Spohn, and M. Kulkarni, Robustness of kardar-parisi-zhang scaling in a classical integrable spin chain with broken integrability (2022), [arXiv:2205.03858](https://arxiv.org/abs/2205.03858).
- [17] M. Ljubotina, M. Žnidarič, and T. Prosen, A class of states supporting diffusive spin dynamics in the isotropic heisenberg model, *Journal of Physics A: Mathematical and Theoretical* **50**, 475002 (2017).
- [18] Žiga Krajinik, E. Ilievski, and T. Prosen, Integrable matrix models in discrete space-time, *SciPost Phys.* **9**, 038 (2020).
- [19] B. Ye, F. Machado, J. Kemp, R. B. Hutson, and N. Y. Yao, Universal kardar-parisi-zhang dynamics in integrable quantum systems, *Phys. Rev. Lett.* **129**, 230602 (2022).
- [20] M. Prähofer and H. Spohn, Exact scaling functions for one-dimensional stationary kpz growth, *Journal of Statistical Physics* **115**, 255 (2004).
- [21] V. B. Bulchandani and C. Karrasch, Subdiffusive front scaling in interacting integrable models, *Phys. Rev. B* **99**, 121410 (2019).
- [22] M. Dupont and J. E. Moore, Universal spin dynamics in infinite-temperature one-dimensional quantum magnets, *Phys. Rev. B* **101**, 121106 (2020).
- [23] F. Weiner, P. Schmitteckert, S. Bera, and F. Evers, High-temperature spin dynamics in the heisenberg chain: Magnon propagation and emerging kardar-parisi-zhang scaling in the zero-magnetization limit, *Phys. Rev. B* **101**, 045115 (2020).
- [24] O. K. Diessel, S. Diehl, and A. Chiochetta, Emergent kardar-parisi-zhang phase in quadratically driven condensates, *Phys. Rev. Lett.* **128**, 070401 (2022).
- [25] M. M. Oliveira, P. Ribeiro, and S. Kirchner, Efficient quantum information probes of nonequilibrium quantum criticality, *npj Quantum Information* **9**, 6 (2023).
- [26] S. Nandy, Z. Lenarčič, E. Ilievski, M. Mierzejewski, J. Herbrych, and P. Prelovšek, Spin diffusion in perturbed isotropic heisenberg spin chain (2022), [arXiv:2211.17181](https://arxiv.org/abs/2211.17181).
- [27] A. Scheie, N. E. Sherman, M. Dupont, S. E. Nagler, M. B. Stone, G. E. Granroth, J. E. Moore, and D. A. Tennant, Detection of kardar–parisi–zhang hydrodynamics in a quantum heisenberg spin-1/2 chain, *Nature Physics* **17**, 726 (2021).
- [28] Q. Fontaine, D. Squizzato, F. Baboux, I. Amelio, A. Lemaître, M. Morassi, I. Sagnes, L. Le Gratiet, A. Harouri, M. Wouters, I. Carusotto, A. Amo, M. Richard, A. Minguzzi, L. Canet, S. Ravets, and J. Bloch, Kardar–parisi–zhang universality in a one-dimensional polariton condensate, *Nature* **608**, 687 (2022).
- [29] D. Wei, A. Rubio-Abadal, B. Ye, F. Machado, J. Kemp, K. Srakaew, S. Hollerith, J. Rui, S. Gopalakrishnan, N. Y. Yao, I. Bloch, and J. Zeiher, Quantum gas microscopy of kardar-parisi-zhang superdiffusion, *Science* **376**, 716 (2022).
- [30] S. Gopalakrishnan and R. Vasseur, Kinetic theory of spin diffusion and superdiffusion in xxz spin chains, *Phys. Rev. Lett.* **122**, 127202 (2019).
- [31] E. Ilievski, J. De Nardis, S. Gopalakrishnan, R. Vasseur, and B. Ware, Superuniversality of superdiffusion, *Phys. Rev. X* **11**, 031023 (2021).
- [32] V. B. Bulchandani, S. Gopalakrishnan, and E. Ilievski, Superdiffusion in spin chains, *Journal of Statistical Mechanics: Theory and Experiment* **2021**, 084001 (2021).
- [33] Žiga Krajinik, E. Ilievski, and T. Prosen, Absence of normal fluctuations in an integrable magnet, *Phys. Rev. Lett.* **128**, 090604 (2022).
- [34] J. D. Nardis, S. Gopalakrishnan, and R. Vasseur, Non-linear fluctuating hydrodynamics for kpz scaling in isotropic spin chains (2023), [arXiv:2212.03696](https://arxiv.org/abs/2212.03696) [[cond-mat.quant-gas](https://arxiv.org/abs/2212.03696)].
- [35] Žiga Krajinik, E. Ilievski, and T. Prosen, Universal distributions of magnetization transfer in integrable spin chains (2023), [arXiv:2303.16691](https://arxiv.org/abs/2303.16691) [[cond-mat.stat-mech](https://arxiv.org/abs/2303.16691)].
- [36] T. Prosen and M. Žnidarič, Diffusive high-temperature transport in the one-dimensional hubbard model, *Phys. Rev. B* **86**, 125118 (2012).
- [37] M. Fava, B. Ware, S. Gopalakrishnan, R. Vasseur, and S. A. Parameswaran, Spin crossovers and superdiffusion in the one-dimensional hubbard model, *Phys. Rev. B* **102**, 115121 (2020).
- [38] M. Imada, A. Fujimori, and Y. Tokura, Metal-insulator transitions, *Rev. Mod. Phys.* **70**, 1039 (1998).
- [39] B. S. Shastry, Exact integrability of the one-dimensional hubbard model, *Phys. Rev. Lett.* **56**, 2453 (1986).
- [40] H. Grosse, The symmetry of the hubbard model, *Letters in Mathematical Physics* **18**, 151 (1989).
- [41] S. Moudgalya, N. Regnault, and B. A. Bernevig, η -pairing in hubbard models: From spectrum generating algebras to quantum many-body scars, *Phys. Rev. B* **102**, 085140 (2020).
- [42] C. P. Moca, M. A. Werner, O. Legeza, T. Prosen, M. Kormos, and G. Zaránd, Simulating lindbladian evolution

- with non-abelian symmetries: Ballistic front propagation in the $su(2)$ hubbard model with a localized loss, *Phys. Rev. B* **105**, 195144 (2022).
- [43] P. J. H. Denteneer, R. T. Scalettar, and N. Trivedi, Particle-hole symmetry and the effect of disorder on the mott-hubbard insulator, *Phys. Rev. Lett.* **87**, 146401 (2001).
- [44] J. Carlström, Spin-charge transformation of lattice fermion models: duality approach for diagrammatic simulation of strongly correlated systems, *Journal of Physics: Condensed Matter* **29**, 385602 (2017).
- [45] D. Jakubczyk, Application of the schur–weyl duality in the one-dimensional hubbard model, *Reports on Mathematical Physics* **85**, 293 (2020).
- [46] M. Ogata and H. Shiba, Bethe-ansatz wave function, momentum distribution, and spin correlation in the one-dimensional strongly correlated hubbard model, *Phys. Rev. B* **41**, 2326 (1990).
- [47] P. Schlottmann, Exact results for highly correlated electron systems in one dimension, *International Journal of Modern Physics B* **11**, 355 (1997).
- [48] X.-W. Guan, M. T. Batchelor, and C. Lee, Fermi gases in one dimension: From bethe ansatz to experiments, *Rev. Mod. Phys.* **85**, 1633 (2013).
- [49] M. Am-Shallem, A. Levy, I. Schaefer, and R. Kosloff, Three approaches for representing lindblad dynamics by a matrix-vector notation (2015), [arXiv:1510.08634](https://arxiv.org/abs/1510.08634).
- [50] A. A. Dzhioev and D. S. Kosov, Super-fermion representation of quantum kinetic equations for the electron transport problem, *The Journal of Chemical Physics* **134**, 044121 (2011).
- [51] M. Jiang, S. Luo, and S. Fu, Channel-state duality, *Phys. Rev. A* **87**, 022310 (2013).
- [52] S. R. White and A. E. Feiguin, Real-time evolution using the density matrix renormalization group, *Phys. Rev. Lett.* **93**, 076401 (2004).
- [53] F. Verstraete, V. Murg, and J. Cirac, Matrix product states, projected entangled pair states, and variational renormalization group methods for quantum spin systems, *Advances in Physics* **57**, 143 (2008).
- [54] U. Harbola and S. Mukamel, Superoperator nonequilibrium green’s function theory of many-body systems; applications to charge transfer and transport in open junctions, *Physics Reports* **465**, 191 (2008).
- [55] A. A. Dzhioev and D. S. Kosov, Nonequilibrium perturbation theory in liouville–fock space for inelastic electron transport, *Journal of Physics: Condensed Matter* **24**, 225304 (2012).
- [56] M. A. Werner, C. P. Moca, O. Legeza, and G. Zaránd, Quantum quench and charge oscillations in the $su(3)$ hubbard model: A test of time evolving block decimation with general non-abelian symmetries, *Phys. Rev. B* **102**, 155108 (2020).
- [57] G. Vidal, Efficient classical simulation of slightly entangled quantum computations, *Phys. Rev. Lett.* **91**, 147902 (2003).
- [58] G. Vidal, Efficient simulation of one-dimensional quantum many-body systems, *Phys. Rev. Lett.* **93**, 040502 (2004).
- [59] F. Verstraete, J. J. García-Ripoll, and J. I. Cirac, Matrix product density operators: Simulation of finite-temperature and dissipative systems, *Phys. Rev. Lett.* **93**, 207204 (2004).
- [60] M. Cheneau, P. Barmettler, D. Poletti, M. Endres, P. Schauß, T. Fukuhara, C. Gross, I. Bloch, C. Kollath, and S. Kuhr, Light-cone-like spreading of correlations in a quantum many-body system, *Nature* **481**, 484 (2012).
- [61] C. Gogolin and J. Eisert, Equilibration, thermalisation, and the emergence of statistical mechanics in closed quantum systems, *Reports on Progress in Physics* **79**, 056001 (2016).
- [62] L. Piroli, J. De Nardis, M. Collura, B. Bertini, and M. Fagotti, Transport in out-of-equilibrium xxz chains: Nonballistic behavior and correlation functions, *Phys. Rev. B* **96**, 115124 (2017).
- [63] Y. Nozawa and H. Tsunetsugu, Generalized hydrodynamic approach to charge and energy currents in the one-dimensional hubbard model, *Phys. Rev. B* **101**, 035121 (2020).
- [64] Y. Nozawa and H. Tsunetsugu, Generalized hydrodynamics study of the one-dimensional hubbard model: Stationary clogging and proportionality of spin, charge, and energy currents, *Phys. Rev. B* **103**, 035130 (2021).
- [65] V. Gorini, A. Kossakowski, and E. C. G. Sudarshan, Completely positive dynamical semigroups of n -level systems, *Journal of Mathematical Physics* **17**, 821 (1976).
- [66] G. Lindblad, On the generators of quantum dynamical semigroups, *Communications in Mathematical Physics* **48**, 119 (1976).
- [67] T. Prosen, Third quantization: a general method to solve master equations for quadratic open fermi systems, *New Journal of Physics* **10**, 043026 (2008).
- [68] A. J. McRoberts, T. Bilitewski, M. Haque, and R. Moessner, Anomalous dynamics and equilibration in the classical heisenberg chain, *Phys. Rev. B* **105**, L100403 (2022).